Characterising the chemical and physical properties of phase-change nanodroplets

Weiqi Zhang [a], Hilde Metzger [b], Stavros Vlatakis [a], Amelia Claxton [a], M. Alejandra Carbajal [c], Leong Fan Fung [d], James Mason [a], K.L. Andrew Chan [a], Antonios N. Pouliopoulos [d], Roland A. Fleck [c], Paul Prentice [b], Maya Thanou [a,*]

[a] *Institute of Cancer & Pharmaceutical Sciences, King's College London, United Kingdom*
[b] *School of Engineering, University of Glasgow, United Kingdom*
[c] *Centre for Ultrastructural Imaging, King's College London, United Kingdom*
[d] *Department of Surgical & Interventional Engineering, King's College London, United Kingdom*

A B S T R A C T

Phase-change nanodroplets have attracted increasing interest in recent years as ultrasound theranostic nanoparticles. They are smaller compared to microbubbles and they may distribute better in tissues (*e.g.* in tumours). They are composed of a stabilising shell and a perfluorocarbon core. Nanodroplets can vaporise into echogenic microbubbles forming cavitation nuclei when exposed to ultrasound. Their perfluorocarbon core phase-change is responsible for the acoustic droplet vaporisation. However, methods to quantify the perfluorocarbon core in nanodroplets are lacking. This is an important feature that can help explain nanodroplet phase change characteristics. In this study, we fabricated nanodroplets using lipids shell and perfluorocarbons. To assess the amount of perfluorocarbon in the core we used two methods, ^{19}F NMR and FTIR. To assess the cavitation after vaporisation we used an ultrasound transducer (1.1 MHz) and a high-speed camera. The ^{19}F NMR based method showed that the fluorine signal correlated accurately with the perfluorocarbon concentration. Using this correlation, we were able to quantify the perfluorocarbon core of nanodroplets. This method was used to assess the content of the perfluorocarbon of the nanodroplets in solutions over time. It was found that perfluoropentane nanodroplets lost their content faster and at higher ratio compared to perfluorohexane nanodroplets. The high-speed imaging indicates that the nanodroplets generate cavitation comparable to that from commercial contrast agent microbubbles. Nanodroplet characterisation should include perfluorocarbon concentration assessment as critical information for their development.

1. Introduction

Microbubbles based on lipids are widely used in the clinic as FDA/EMA approved ultrasound contrast agents (UCAs) [1]. Microbubbles can have linear and nonlinear oscillation upon exposure to ultrasound which can be used to enhance the diagnostic ultrasound signal, in addition, the oscillation behaviour can also be used in therapeutic applications, *e.g,* drug/gene delivery [2], tumour ablation [3], and blood-brain barrier opening[4]. However, microbubbles have limitations due to their relatively large size (typically 3–10 μm) and unstable gas core [5]. Microbubbles can only be used intravascularly because their microscale size prevents them from extravasating out of the vasculature [5]. Microbubbles also have short *in vivo* circulation time (*e.g.* minutes) due to the rapid loss of their gaseous core through their shell in blood [6,7]. Therefore, to overcome these problems, phase-change nanodroplets (PCND) have been developed over the last two decades. PCNDs, also known as nanodroplets (NDs), may be defined as nano-sized

nanoparticles with a liquid perfluorocarbon (PFC) core which can be used as UCAs [8]. Once exposed to sufficient ultrasound energy, NDs can vaporise to form highly echogenic microbubbles. PCND sizes are below 1 μm which allows them to form much more homogenous suspensions compared to their microbubble counterparts [9]. The core of PCNDs can remain liquid in circulation which improves their half-life to a few hours, increasing both their contrast enhancement and therapeutic potential [10,11]. Small sized PCNDs would allow better distribution around cancerous lesions which could lead to more uniform contrast enhancement [12]. Further, their small size would allow them to permeate through the vascular endothelial wall and reach target tissue sites, like tumours [13].

NDs are composed of an encapsulating shell and a triggerable phase-change (liquid-to-gas) core [14]. The physicochemical and biological properties of PFCs make them a desirable component for the phase change core of NDs as they are bioinert and can be excreted *via* the lungs after being released into the blood stream [15,16]. Their appropriate

boiling point allows PCNDs to undergo acoustic droplet vaporisation (ADV) under ultrasonic exposure of sufficient intensity. The Laplace pressure provided by the shell allows them to stably circulate in the body until activation [17]. Since the PFC family have a range of compounds with different boiling points, the core composition can be adjusted to the desired ADV properties. For example, NDs with low-boiling point PFCs will vaporise at lower intensities, therefore they are suitable for diagnostic applications as UCAs [18]. Rapoport *et al.* showed that NDs with perfluorocarbon ether (PFCE, $C_{10}F_{20}O_5$) core have greater storage ability than NDs with dodecafluoropentane (DDFP, C_5F_{12}) core, because PFCE has a much higher boiling point (146 °C) than DDFP (29 °C) [19]. It is likely that the lower boiling point of DDFP was not well contained within the NDs leading to poor storage stability. On the other hand, PFCE NDs required slightly higher acoustic intensity to vaporise compared to the DDFP NDs. This indicates the balance is required between the PFC core choice and the applied ultrasound intensity. Melich *et al.* also showed that increasing the perfluorohexane (PFH)/perfluoropentane (PFP) ratio in the PFH/PFP mixture core increases the ADV threshold of NDs [20]. Apart from the PFC core, the shell material is also an important component for NDs. The shell should provide sufficient Laplace pressure for NDs to maintain their core in the liquid phase *in vivo*, but at the same time be soft enough to support deformation during ADV and cavitation [10]. The commonly used shell materials are polymers and lipids. Compared with lipid shelled NDs, their polymer shelled analogues are more rigid and therefore have a higher ADV threshold [15]. In this study, PCNDs made of bio-compatible lipid shell (and thus safe for *in vivo* applications) were are investigated.

Various studies have shown the potential of PCNDs for clinical application, including for targeted drug delivery [21], embolotherapy [22], ultrasound contrast-enhanced imaging [23], tumour ablation [24,25] and histotripsy [26]. Apart from diagnostic and therapeutic studies, the formulation and characterisation of NDs, and the underlying mechanism of ADV and cavitation have also been investigated. There are several commonly used characterisation methods: dynamic light scattering (DLS) was used to investigate colloidal properties [27,28]; the morphology of NDs can be observed using Transmission Electron Microscopy (TEM) [29]; the phase change of droplets to bubbles can be observed optically [30]; *in vitro* acoustic properties of NDs have been investigated using ultrasound. The experimental setup for testing the vaporisation and cavitation processes varies between studies, but is usually composed of three parts: the ultrasound system, the optical system (microscope or camera) and sample container (*e.g.* constraining tube or gel phantom) [9,31]. The factors which may influence the acoustic properties of the NDs have been previously considered in several studies [15]. It has been reported that the ultrasound intensity, frequency and driving amplitude can determine if non-inertial or inertial cavitation from NDs is generated, for different biomedical applications [32]. Both the shell and the core material can influence vaporisation thresholds and cavitation [20,33,34]. Yang *et al.* showed that high droplet concentrations can reduce the difference between ADV and the inertial cavitation threshold [35]. Rojas *et al.* also indicated that boundary constraints and media viscosity can affect ADV threshold [36]. As cavitation is strongly dependent on the PFC core, it is becoming increasingly important to quantify the core content.

However, the current chemical characterisation methods for NDs are limited. Stability studies, for example, are typically conducted with DLS and microscopy, but fail to assess the PFC core content change or loss. As mentioned previously, PFC plays an important role in the ADV and cavitation of NDs. Therefore, it is necessary to develop methods to monitor the PFC change in NDs. In this study, we have developed three formulations of lipid-coated NDs with different perfluorocarbon cores: PFP (boiling point 29 °C), PFH (boiling point 56 °C) and the mixture (volume ratio 1:1) of these two PFCs. The objectives of this study were to develop novel methods to prepare and evaluate NDs, which can be used for further *in vitro* studies and be widely applied in lipid/polymer-coated NDs characterisation. We investigated the size and stability of our

PCNDs preparations, as well as utilised a novel approach to monitor the PFC core content change via ^{19}F NMR. In addition, we explored the cavitation behaviour of the NDs using high-speed imaging during ultrasound exposure and compared to equivalent observations for commercial contrast agent microbubbles.

2. Materials & methods

2.1. Materials

Perfluoropentane and perfluorohexane were purchased from Apollo Scientific Ltd (UK). De 1,2-Dipalmitoyl-*sn*-glycero-3-phosphocholine (DPPC; 16:0 PC), and (ω-methoxy- polyethyleneglycol$_{2000}$)-N-carboxy-1,2-distearoyl-*sn*-glycero-3-phosphoethanolamine (DSPE–PEG(2000)) were purchased from Avanti Polar Lipids (AL, USA) or Sigma Aldrich (MO, USA). Other materials were from Sigma-Aldrich and were of analytical grade. The standard buffers were sterile 20 mM HEPES, 5% (w/v) d-glucose corrected to pH 7.4. Sonazoid® microbubbles were purchased from GE Healthcare (Oslo, Norway).

2.2. Preparation of NDs

NDs were prepared with the following lipid formation molar ratio; DPPC: DSPE-PEG(2000) 93:7 (mol%, 30 mg total lipid, per batch). All lipids were dissolved in chloroform and mixed in a round bottom flask at room temperature in the appropriate proportions. The solvent was then removed using a rotary evaporator and the resulting film dried overnight *in vacuo*, forming an even and thin lipidic film. All buffers were sterilised by filtration through 0.2 μm membranes and degassed using Degassing Station (TA Instruments, New Castle, DE, USA) for 1 h. Dried lipid film was hydrated with 1 mL filtered buffer (20 mM HEPES aq. with 5 w% glucose; pH 7.4), and sonicated using 90 W sonicator at 45–50 °C for 3–5 min. Suspension was transferred to a 2 mL glass vial, additional 1 mL buffer was added to vial so it was nearly full, and the vial was sealed and cooled on ice. 1% v/v PFC was added to the suspension (the pipette tips should go below the solution surface to avoid loss of PFC) and the vial sealed immediately (the added PFC formed a droplet at the bottom of the vial because PFC have higher density than aqueous buffer). The mixture was then vortexed aggressively (using vortex mixture at 3200 rpm) for 20 s to emulsify the PFC, and cold sonicated (using 90 W sonicator) for 3 to 5 min. The procedure was repeated 2–3 times, until a milky suspension and no obvious PFC droplets remained at the bottom of the vial. The cold sonication was continued for a further 30–60 min to produce a cloudy suspension. The ND suspensions were stored under seal in fridge at 5 °C. For Dil fluorescence labelled NDs, the same method was used except for the formulation: (DPPC: DSPE-PEG(2000): Dil 92.99:7:0.01 mol%, 30 mg total lipid, per batch).

2.3. Preparation of liposomes

Lipsosomes were prepared with the following lipid formation molar ratio; DPPC: DSPE-PEG(2000) 93:7 (mol%, 30 mg total lipid, per batch). All lipids were mixed in a round bottom flask at room temperature in the appropriate proportions. The solvent was then removed using a rotary evaporator and the resulting film dried overnight *in vacuo*, forming an even and thin lipidic film. All buffers were sterilised by filtration through 0.2 μm membranes. Dried lipid film was hydrated with 1 mL filtered buffer (20 mM HEPES aq. with 5 w% glucose; pH 7.4), and sonicated at 45–50 °C for 30 min until form homogenies liposome solution.

2.4. Colloidal properties

ND size and population parameters for each batch were routinely recorded by dynamic light scattering (DSL) using a Nanoseries Nano ZS

(Malvern Panalytical, UK). Samples were diluted 1:20 v/v using storage buffer at 25 °C and contained in disposable micro-cuvettes. Analysis was repeated in triplicate and size modelling carried out using default solute and particle parameters. Surface charge (ζ potential) measurements were also carried out on representative batches at 1:10 v/v dilution, using default settings and 3 repeats.

2.5. Differential scanning calorimetry (DSC)

Differential scanning calorimetry was used to assess the NDs phase transition. NDs were diluted to around 1.5 mg/mL lipid into degassed 20 mM HEPES, 5 % w/v glucose buffer, pH 7.4. Samples (600 μL) were then loaded into a Nano DSC (TA Instruments, New Castle, DE, USA) and three rounds of sequential heating/cooling (25–70 °C at 1 °C/min) were then performed against a reference of the same buffer. Each scan sequence was carried out in triplicate.

2.6. ^{19}F NMR spectroscopy

1D (one dimensional) experiments were conducted on a Bruker AVANCE NEO 600 spectrometer equipped with a proton optimized triple resonance NMR inverse probe operating at a Larmor frequency of 564 MHz for ^{19}F. Temperature setting was 278–283 K and number of scans was 32 scans. NMR data were processed using Topspin 4.1.4 and MestReNova Lite CDE.

2.7. Sample preparation for ^{19}F NMR

Buffer solution saturated with PFP was prepared by adding 50 μL PFP into 2 mL HEPEPS buffer. The PFP formed a droplet at the bottom of the vial. The vial was sealed and sonicated for 10 mins in ice bath until the suspension became cloudy. The cloudy suspension was stored in fridge (5 °C) overnight and the supernatant became clear. The saturated PFP supernatant solution was collected. The supernatant was then diluted x10 times using a D_2O:TFA (Trifluoroacetic acid) solution (1:1*10^{-3} % v/v TFA as internal standard) before ^{19}F NMR measurement.

The PCNDs were also diluted x10 times using the same D_2O:TFA solution as above before ^{19}F NMR measurements were carried out to prove the PFC signal on ^{19}F NMR spectrum originated from the core of the NDs. To establish a calibration curve, NDs with a known amount of PFC (the amount of PFC added during NDs preparation were weighed using an analytical balance) were serially diluted with D_2O and the area of the ^{19}F NMR peaks was plotted against PFC concentration.

2.8. Fourier-transform infrared (FTIR) spectroscopy

20 μL of sample were placed in liquid cell before FTIR spectrometer (Tensor II, Bruker Optics) measurement. All measurements were acquired with a spectral resolution of 8 cm^{-1} and a spectral range of 4000 to 800 cm^{-1}, over 16 scans.

2.9. Thermal effect of NDs

The experimental setup is shown in SI Fig. S1. ND samples (5× dilution with degassed buffer solution) were contained in a single-dimple microscope slide, sealed with a cover glass and placed on black card. A thermocycler was used as a heat block and monitored using a thermocouple. LED lights were set at a low angle on top of the sample. A blackfly video camera without filters, was focused on the ND layer and recorded data was safely stored. ND samples were heated at various temperatures for 5 min, with the camera set to 1 fps to track the evolution of gas bubbles. Heating curves were collected from a thermocouple placed just underneath the slide. Images were processed *via* ImageJ.

## 2.10. Imaging of cavitation using high-speed camera

All experimental observations were performed inside a bespoke 420×438×220 mm^3 cavitation tank, filled with de-ionised and degassed water. A 90 mm diameter transducer (H-198, Sonic Concepts) was excited by a power amplifier (1040L, E&I), driven for 100 cycles at 1.1 MHz by an arbitrary waveform generator (DG4102, Rigol). A 500 μm polycarbonate capillary (Paradigm Optics) was situated in the centre of the ultrasound focal region via a custom 3D printed mount, with the capillary inlet and outlet secured via epoxy to silicon tubing. NDs were diluted around 50 times in degassed water (through boiling and sealed cooling) and flowed through the capillary from a syringe with a 20G microlance, inserted into the bore of the silicon tubing inlet. The silicon tubing outlet vented to a collection reservoir outside of the tank. A high-speed camera (HPV-X, Shimadzu), and a 5× objective lens, focused on the interstection of the ultrasound focus and the capillary, captured cavitation dynamics at $10×10^6$ frames per second (fps), over a duration of 25.5 μs. The imaging was triggered using a pulse delay generator (DG535, Stanford Research) 51.6 μs after the transducer was excited, to allow for the ultrasound to propagate from the transducer to the capillary. Illumination was provided from below via a liquid light guide using synchronous 10 ns laser pulses (CAVILUX, Cavitar). To ensure the ultrasound focus was positioned correctly in the high-speed imaging with a macro-lens was used as shown in Fig. 1 [37].

2.11. Passive cavitation detection (PCD)

To investigate the acoustic response of these NDs, a 7.5 MHz passive cavitation detector (Part no. U8423539, V320, diameter: 12.7 mm, focal depth: 76.2 mm; Olympus Industrial, Waltham, MA, USA) was used to collect acoustic emissions, which was inserted and co-aligned with the FUS transducer, having overlapping foci. A 1.5 MHz spherical-segment single-element FUS transducer (Part No. H-195; Sonic Concepts, Bothell, WA, USA) was driven by a waveform generator (33500B series; Keysight technologies, Santa Clara, CA, USA) through a 50 dB radio-frequency power amplifier (Model A075; E&I, Rochester, NY, USA). A low-density polyethylene tube (inner diameter: 0.4 mm, outer diameter: 0.8 mm; Fisher Scientific, UK) was fixed using a stand and then submerged in a de-ionised water container (SI Fig. S2). A raster scan was performed to locate the channel along the lateral and elevational dimensions. The focal volume (0.7 mm × 3.8 mm) was placed at the centre of the channel along the axial dimension, using pulse echo. Control sonications were conducted with degassed buffer flowing at a constant velocity of 10 mm/s in order to imitate capillary flow. Finally, NDs were diluted to 1.5 mg/mL (lipid concentration) in degassed buffer and were made to flow at the same fluid velocity as control (sentence before this one says that degassed buffer was used as a control). A total of 100 pulses were emitted per amplitude condition and acoustic emissions were captured by the passive cavitation detector. For each ND formulation, the following ultrasound parameters were used: 1.5 MHz, 5 Hz Pulse repetition frequency (PRF), 1500 cycles, 200 kPa- 1500 kPa (50 kPa increments). Acoustic cavitation emissions were processed offline in MATLAB. Measurements are presented as mean ± standard deviation [38].

2.12. Transmission electron microscope (TEM)

For transmission electron microscope (TEM) analysis, a drop (3 μL) of the NDs sample (lipid concentration 0.3 mg/ml) was deposited onto glow discharged 300-mesh copper grids with carbon support film (Electron Microscopy Sciences, Cat No. 71150) and allowed to adhere (30 sec). Grids were then briefly washed in a drop of aqueous uranyl acetate (3% w/v), lightly blotted on filter paper and immediately placed onto a second drop of aqueous uranyl acetate (1 min). Grids were wicked to dryness and allowed to air-dry before viewing using a TEM operated at 80 kV (JEOL JEM 1400Flash, JEOL, Japan). Images were acquired
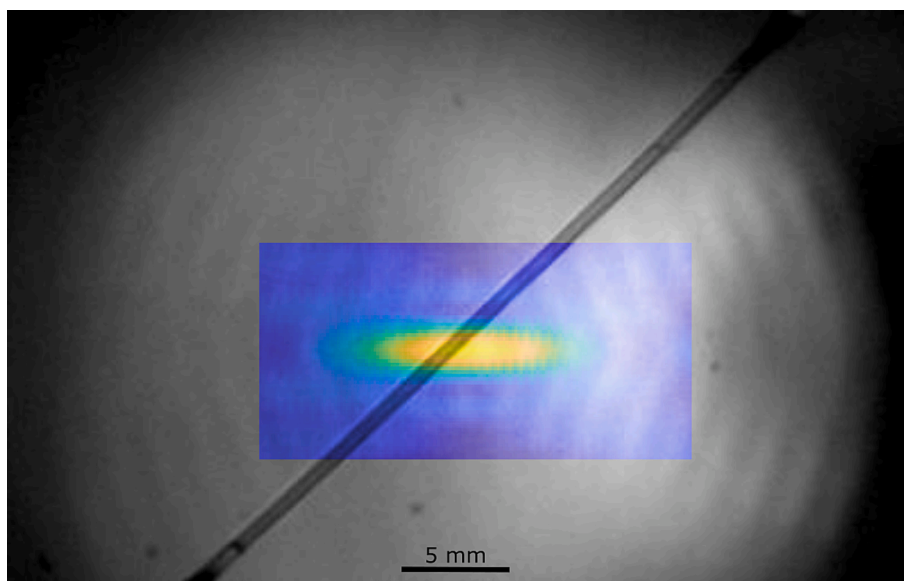
Fig. 1. Shadowgraphic imaging of the ultrasound field with a hydrophone scan of the focal region is overlaid. The capillary was positioned through the focus at 45°. Full image sequence of field imaging is available as SI (Video SV1).

with a 2 k by 2 k format CCD camera (JEOL Flash CCD Camera, JEOL, Japan). A similar method has previously been used to characterise lipid-based nanoparticles[39].

3. Results and discussion

3.1. Optimising the method of preparation of the lipid shell NDs

In this study we prepared NDs following a modified bath sonication protocol as previously described by Gao *et al.*[40] and Sheeran *et al.* [41]. In short, the lipids dissolved in organic solvents were combined and dried *in vacuo* to make a thin lipid film. The lipid film (shell material) was initially first hydrated with HEPES buffer and hot sonicated (45 °C) until formation of a cloudy lipid suspension (SI Fig. S3). The suspension was then cooled in ice prior to the addition of the PFC as excess heat may cause vaporisation and subsequent loss of PFC. The PFC was then added to the vial (ensuring no gap between the solution surface and the cap). The vial was tightly sealed and cold sonicated until NDs were formed.

In previous studies by Sheeran *et al.* and Ferri *et al.*, NDs were they prepared NDs using either bath sonication or high intensity tip sonication [30,41], which are simple and inexpensive techniques[15]. We choose bath sonication instead of tip sonication because erosion of the probe tip has the potential to contaminate NDs with potentially toxic metals during preparation [41]. It has been reported that NDs fabricated by sonication have higher size polydispersity compared with those fabricated by microfluidics [41]. However, the benefit of as all components are contained in one vial/flask reducing the loss of both shell and core material throughout the preparation process, outweighed the potentially higher PDI [15]. To maximise the reproducibility of this preparation process, the sonication conditions *e.g.* temperature and vial volume were controlled to provide NDs with a satisfactory size (around 110 nm diameter) and PDI (Poly-Dispersity Index; <0.25).

3.2. Effect of increasing perfluorocarbon content in the NDs

PFC content (%v/v) may influence ND properties. Previous studies have demonstrated that any volume of liquid PFCs that were not encapsulated in droplets would sediment [10]. Therefore, it is important to choose an appropriate amount of PFCs during preparation. First, we studied the influence of PFC volumetric percentage. We have prepared

two formulations of NDs with 1% v/v (MIX1ND) and 2% v/v (MIX2ND) mixture of PFC (1:1 PFP:PFH) as their core. A previous study has shown that increasing the amount of PFC could increase ND diameter due to a corresponding decrease in the concentration of shell material, relative to the amount of PFC[30].

As expected, and in agreement to the previous data, increasing the volume of PFC from 1% v/v to 2% v/v led to an increase of average size from 107.0±2.4 nm to 204.8±0.6 nm (Fig. 2c). To quantify the PFC content, we used ^{19}F NMR. ^{19}F NMR data also confirmed that MIX2ND have two times higher amount of PFC than MIX1ND (SI Fig. S4) [30]. After a few days in storage (5 °C), the size of both NDs decreased, but MIX2ND decreased at a higher rate (Fig. 3d). When MIX2ND were stored in the fridge for 3–4 days, there was a white precipitate at the bottom of the vial (Fig. 2b). To investigate whether this precipitate originated from the lipid shell or the PFC core, we prepared NDs with the same lipid composition but added DiI fluorescence dye (1,1′-Dioctadecyl-3,3,3′,3′-Tetramethylindocarbocyanine Perchlorate, Fig. 2a). DiI intercalates into the lipid shell providing a fluorescence/optical indication of the location of the lipids [42]. We observed that the colour of the precipitate continued to be white for the DiI-labelled NDs, which indicated that sedimentation originated from the PFC core rather than the lipid shell (SI Figs. S5 and S6). Therefore, for the rest of the tests we prepared NDs with 1% v/v of PFC.

3.3. Effect of using different type of perfluorocarbon core

The PFC family differs in chain length, which leads to different boiling points [17]. NDs with different PFC core were also expected to have different properties. We conducted several tests to investigate ND with three different cores: 1% v/v PFP (PFP1ND), 1% v/v PFH (PFH1ND) and 1% v/v mixture (1:1 PFP:PFH, MIX1ND).

The average sizes of three NDs were similar, which were 106.4±3.6 nm, 107.0±2.4 nm and 109.6±3.3 for PFP1ND, MIX1ND and PFH1ND respectively (Fig. 3a). Previous literature demonstrated that NDs size are submicrometer at around 100 to 500 nm [41,43]. Whereas our NDs have a smaller size (around 100 nm) and a tighter size distribution (SD ± 2–4 nm) compared with distributions detailed in previous literature (SD ± 9–100 nm) [6,30]. The ζ-potential for PFP1ND, MIX1ND and PFH1ND were −14.43±0.54 mV, −15.83±0.65 mV and −17.73±0.39 mV respectively (Fig. 3b). To observe the structure of NDs, TEM was performed. The NDs were stored in aqueous solution. However, during TEM
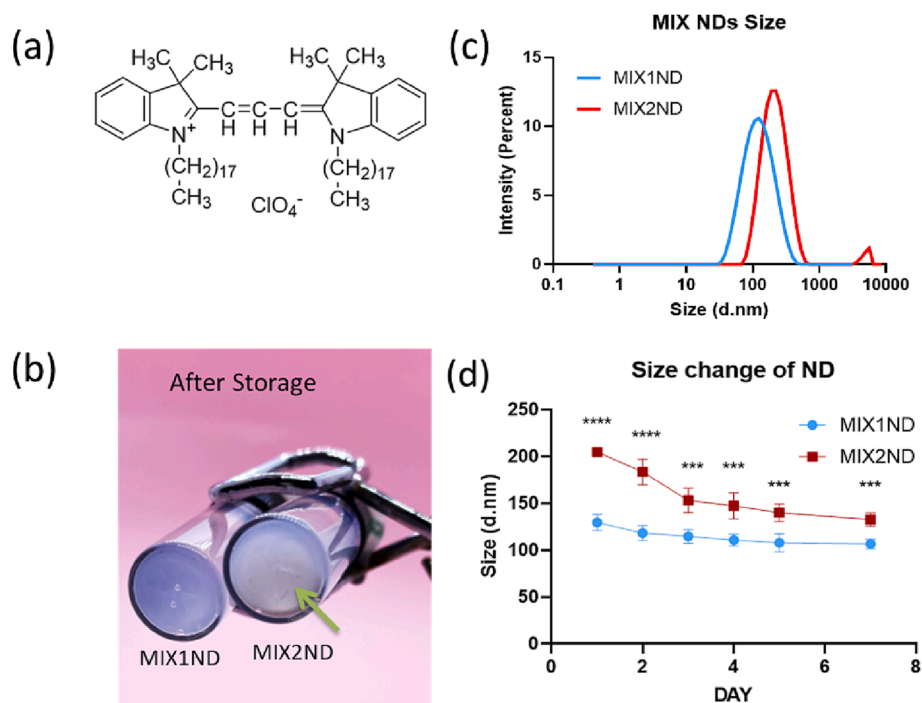
Fig. 2. (a) Chemical structure of Dil (1,1′-Dioctadecyl-3,3,3′,3′-Tetramethylindocarbocyanine Perchlorate); (b) Photo of sample MIX1ND & MIX2ND (Background: pink), MIX2ND have white precipitate after 3 days, as indicated by green arrow (MIX1ND = ND sample with 1% v/v of mixture PFC as core; MIX2ND = ND sample with 2% v/v of mixture PFC as core); (c-d) Effects of volumetric percentage on size property of MIX1ND and MIX2ND; (c) Size distribution of ND; (d) size change of ND stored in fridge. Data in 2d are presented as mean ± SD, n = 3. P value was generated by T-tests between size of different sample on the same day, no significant at P > 0.05 (*P < 0.05, **P < 0.01, ***P < 0.001, and ****P < 0.0001). (For interpretation of the references to colour in this figure legend, the reader is referred to the web version of this article.)
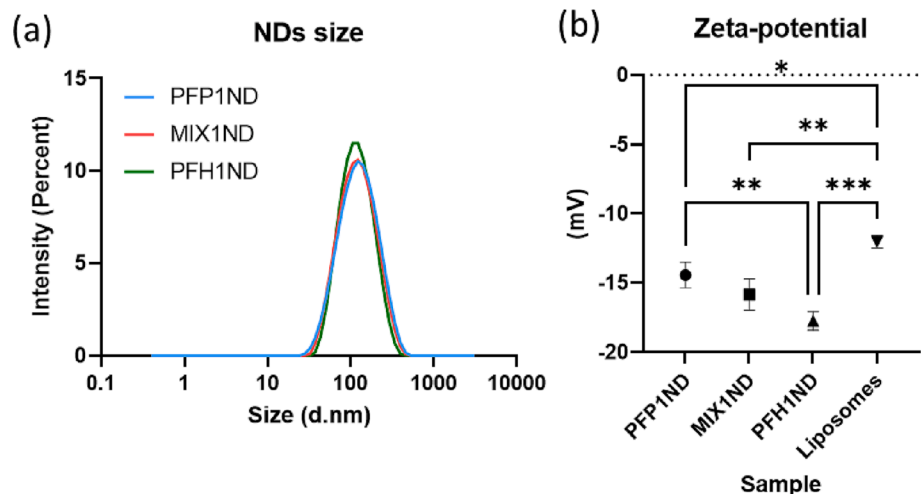

Fig. 3. Colloidal properties of NDs. Effect of PFC core type and composition on (a) ND size and (b) zeta potential. Liposomes were prepared to investigate if all the negative zeta potential was contributed by the PFC core (PFP1ND = ND sample with 1 v/v% PFP as core, MIX1ND = ND sample with 1 v/v% mixture PFC as core, PFH1ND = ND sample with 1% v/v PFH as core, liposomes = liposome with lipid shell composition of DPPC:DSPE-PEG(2000) 93:7, mol%). Data in 3b are presented as mean ± SD, n = 3. P value was generated by one-way ANOVA test, no significant at P > 0.05 (*P < 0.05, **P < 0.01, ***P < 0.001, and ****P < 0.0001).

sample preparation procedure, ND suspensions need to be dried and placed under vacuum which may change the morphology of NDs and cause them to collapse or shrink. All three samples (PFP1ND, MIX1ND and PFH1ND) were spherical in structure (SI Fig. S7). PFH1ND had a relatively higher homogenous structure, which may be due to the high boiling point of its PFH core (56 °C) increasing its stability and thus helping to maintain its structure. Although PFP1ND and MIX1ND samples showed a lower density of integrate NDs and were less homogenous, we were still able to observe spherical structures. The diameter of NDs under TEM is around 70 to 100 nm which is smaller than what we measured under DLS. This is because DLS measured the hydrodynamic diameter of the particles whereas TEM measured the lipid shell diameter.

Behaviour of NDs under increasing temperature was assessed using DSC. DSC thermographs showed all three NDs have three peaks (Fig. 4). During heating process, the shell of NDs melt first and this may cause release of PFC afterwards. The high peak at 42 °C is caused by phase

transition of lipid shell from gel to liquid crystalline phase. The shoulder peak at 44 °C is the melting of the PEG. The peak between 46 and 48 °C was considered to belong to PFC core because liposomes with the same lipid formulation do not have peak above 45 °C. Although PFP and PFH have very different boiling points, they have a similar peak at 46 °C. It is possible that this is the deformation of lipid shell initiates the PFC release from the NDs.

We further examined the behaviour of NDs at different temperatures. When the NDs' core is liquid, the droplets are nanosized and these results in clear solutions as observed by naked eye; but when liquid core becomes gaseous, NDs become micron-sized bubbles, visible to the eye and the number of these bubbles can be counted using a camera. The images with the visible bubbles were processed by ImageJ to count the number of the formed bubbles (SI Fig. S1 and S8). At 25 °C, all three ND samples did not show gas expansion and nearly no bubbles. At 37 °C and 42 °C, both PFP1ND and MIX1ND have developed more bubbles compared to the sample kept at 25 °C. The sample PFH1ND at 37 °C and
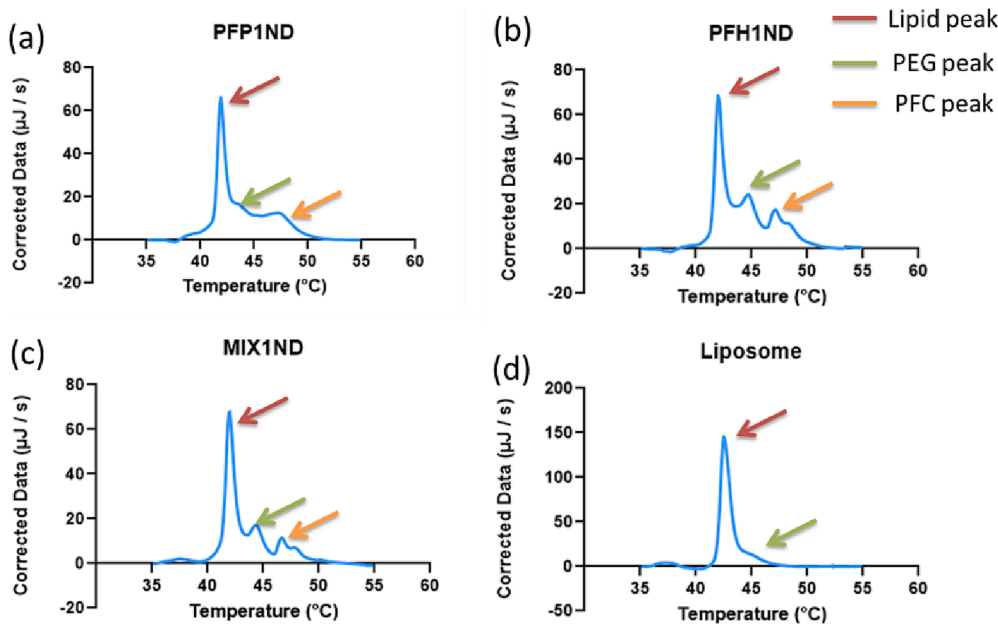
Fig. 4. DSC thermograph of NDs with different cores (a) PFP1ND; (b) PFH1ND; (c) MIX1ND; (d) liposomes with same lipid shell composition (DPPC:DSPE-PEG(2000) 93:7, mol%). Red arrow: DPPC peak, green arrow: PEG peak, orange arrow: PFC peak (PFP1ND = ND sample with 1 v/v% PFP as core, MIX1ND = ND sample with 1 v/v% mixture PFC as core, PFH1ND = ND sample with 1% v/v PFH as core, liposomes = liposome with lipid shell composition of DPPC:DSPE-PEG(2000) 93:7, mol%). (For interpretation of the references to colour in this figure legend, the reader is referred to the web version of this article.)

42 °C showed a low number of bubbles which may be due to the high boiling point of PFH (56 °C). Although NDs can exist in a superheated state due to Laplace pressure provided by their shells, the type of PFC core will still influence the state of NDs under different temperature [44]. The boiling point of PFP is much lower than PFH, therefore the PFP1ND sample produces more bubbles than PFH1ND, at 37 °C and hyperthermic (42 °C) temperatures. To examine whether PFH1ND can evolve to bubbles at PFH boiling point, we heated PFH1ND to 56℃ and observed significant increase in bubble number after 5 mins. We consider this method offers qualitative assessment of the effect of the PFC core rather than offering a quantitative analysis of the accurate numbers of bubbles, but it offers a rough idea about thermal stability of NDs under different temperature. Since PFH NDs produce much less ratio of bubbles at body temperature and hyperthermic temperature, it indicated that PFH NDs will have better thermal stability for future *in vivo* application compared with PFP NDs.

3.4. ^{19}F NMR for the quantification of PFC in NDs

PFC is the key component for NDs cavitation, and cavitation is the main property which makes ND a novel nanoparticle compared with traditional preparations (such as liposomes or micelles). Therefore, it is necessary to develop a method to assess the quantity of PFC in NDs. PFCs are composed of different carbon chain lengths with all other bonds occupied by fluorine. There is no fluorine component in the lipid shell (phospholipids), so we can assume that any ^{19}F NMR signal we measure is due only to the PFC.

First, we compared the ^{19}F NMR signal of PFP saturated HEPES buffer solution with PFP1ND solution. We added TFA (trifluoroacetic acid) in both samples as the internal standard. In these conditions, PFP saturated buffer solution only give signal for the TFA internal standard, whereas the NDs generated a strong carbon-fluorine (C-F) bond signal. This could be because in the NDs solution the hydrophobic PFP is homogenously dispersed in the lipid shell, whereas in the PFP saturated buffer sample, PFP is hydrophobic and thus may have poor solubility in aqueous buffer solution (SI Fig. S9). We proved that ^{19}F NMR could be used to assess the PFC contained by the lipid shell.

Then, we analysed NDs with different cores: PFP1ND, PFH1ND and MIX1ND. Results indicate that ^{19}F NMR could be used to identify PFC type inside NDs, according to the chemical shift and integration number (Fig. 5a – c). All three NDs have a peak at −84 ppm, which was identified

as –CF$_3$ located at the side of carbon-fluorine chain. Other PFC peaks have different chemical shift as they are influenced by the C-F bond. ^{19}F NMR can not only identify PFC type in NDs but could also be used for quantification. We found PFC concentration within the NDs has good correlation with NMR peak area. Then we plotted the ND/PFC concentration versus NMR peak area (Fig. 5d & SI Fig. S10). Both PFP and PFH core ND plots showed an acceptable correlation coefficient ($R^2 > 0.99$). For this study, we only investigated our fabricated lipid shell NDs, but this method also has potential to easily be applied to polymer shell or protein shell NDs because ^{19}F NMR spectra only show signal for fluorine bonds. However, for some fluorinated surfactant formulated NDs, *e.g.* fluorosurfactant-Zonyl®[45], FTAC[27], this method is not applicable because C-F bond from fluorinated surfactant will overlap with the signal generated from the PFC core which may cause interference.

We analysed PFH1ND mixed with Fetal Bovine Serum (FBS) using ^{19}F NMR (SI Fig. S9b). The spectrum gave clear signal of PFH without interference peak, which indicated 19F NMR has the potential to be used for analysis of *in vitro* samples (*e.g.* serum).

3.5. FTIR for the detection and quantification of PFC in NDs

Unlike ^{19}F NMR which only has a peak for a fluorine component, the FTIR spectrum has signals for all chemical bonds. Choi *et al.* used FTIR to detect the PFH in NDs to assess the stability under different temperatures [45]. In this study, when PFH was not added to the NDs, there was no peak on FTIR spectrum between 1300 and 1200 wavenumbers (cm^{-1}). However, after adding PFH, there was a double peak between 1300 and 1200 cm^{-1} [45]. We examined three ND samples on FTIR: PFP1ND, PFH1ND and MIX1ND. The peak between 1300 and 1200 cm^{-1} were identified as C-F bond (Fig. 6a – c, the example of whole spectrum can be found in SI Fig. S11a). We also tested different concentrations of PFH ND and found there is a correlation between PFH concentration and peak absorbance at 1250 cm^{-1} (Fig. 6d & SI Fig. S11b). However, the correlation coefficient is around 0.85, which is lower than R^2 for ^{19}F NMR, so we consider FTIR as a "rough and ready" method for detection and semi-quantification of PFC. Since ND samples with different cores have a different shape of peak between 1300 and 1200 cm^{-1}, FTIR also has the potential to develop "fingerprint" spectrum for identification of PFC inside ND.
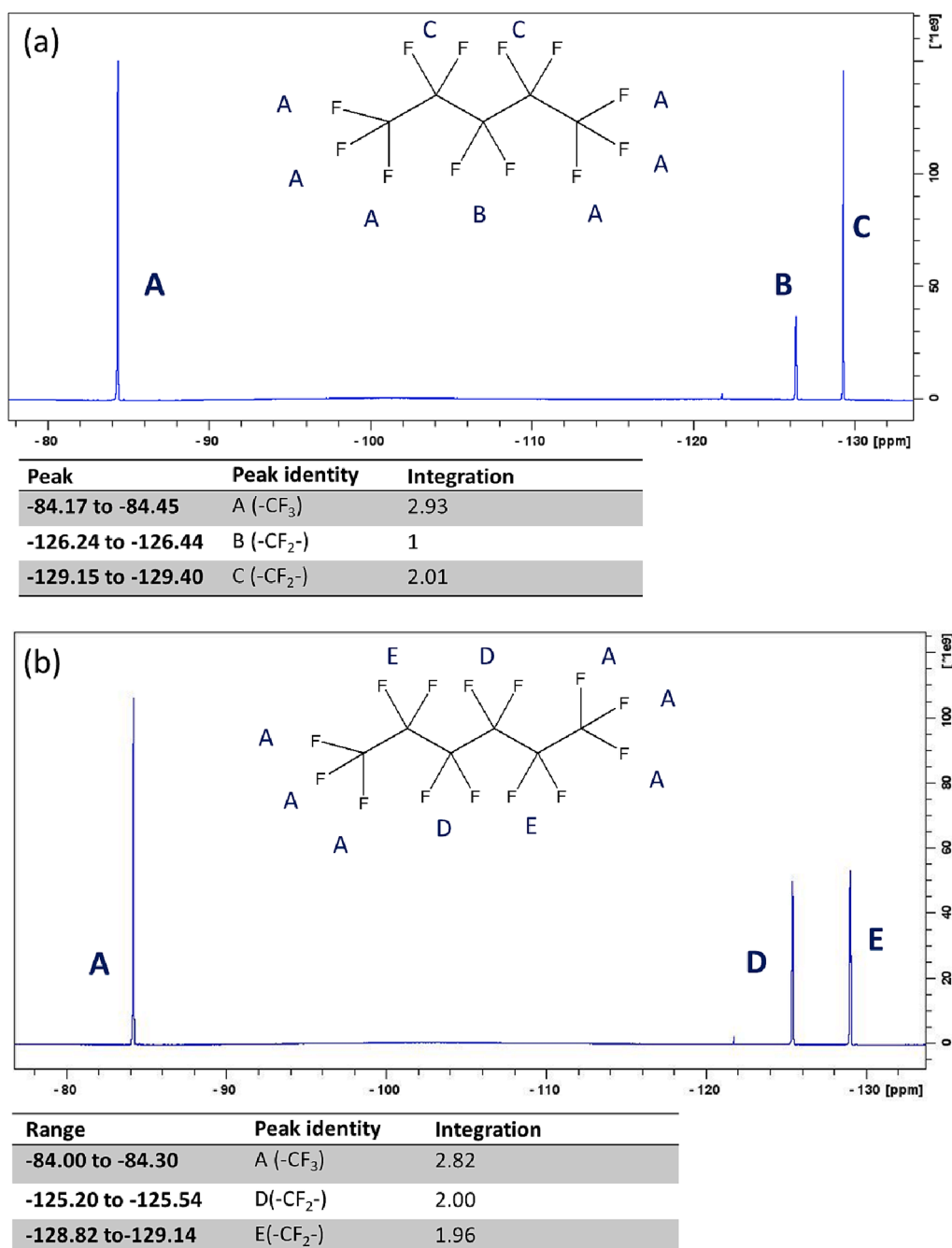
Fig. 5. (a-c) ^{19}F NMR spectrum of NDs and information for chemical shift and integration. (a) PFP1ND, (b) PFH1ND, (c) MIX1ND (PFP1ND = ND sample with 1 v/v % PFP as core, MIX1ND = ND sample with 1 v/v% mixture PFC as core, PFH1ND = ND sample with 1% v/v PFH as core). (d) Correlation between PFH concentration and peak area, peak A: Y = $3.40*10^7$*X R^2 = 0.997; peak D: Y = $2.42*10^7$*X, R^2 = 0.995, peak E: Y = $2.36*10^7$*X, R^2 = 0.996.

3.6. Assess stability of NDs

With all the techniques mentioned above, we can assess the stability of NDs. We tested the size and the amount of PFC change of NDs during refrigeration. Results show that the size of all three NDs decreased during storage and PFP1ND showed more rapid lost compared with PFH1ND (Fig. 7a). This might be caused by leakage of PFC from NDs. To confirm this hypothesis, we quantified the PFC loss using ^{19}F NMR. For the single PFC component NDs, the PFP1ND lost 21.8% of its encapsulated PFC, whereas PFH1ND only lost 7.6% of its encapsulated PFC in 14 days. For the mixed PFP/PFH ND, a total PFC loss of 15.8% was observed (Fig. 7b). We have shown that the PFH cored ND have over two

times better PFC storage stability compared to its PFP analogue. We attribute the rapid loss of PFP vs its PFH analogues due to the lower boiling point of PFP vs PFH, which might increase the leakage from ND and subsequent loss from the formulation due to vaporisation of the PFP. Although FTIR is not that accurate as ^{19}F NMR for quantification, the stability assay was also performed using FTIR to analyse the PFC loss (SI Fig. S12). These data indicate that NDs with PFP core lose significant amount of their PFC content over two weeks period.

3.7. High-speed imaging of ND cavitation

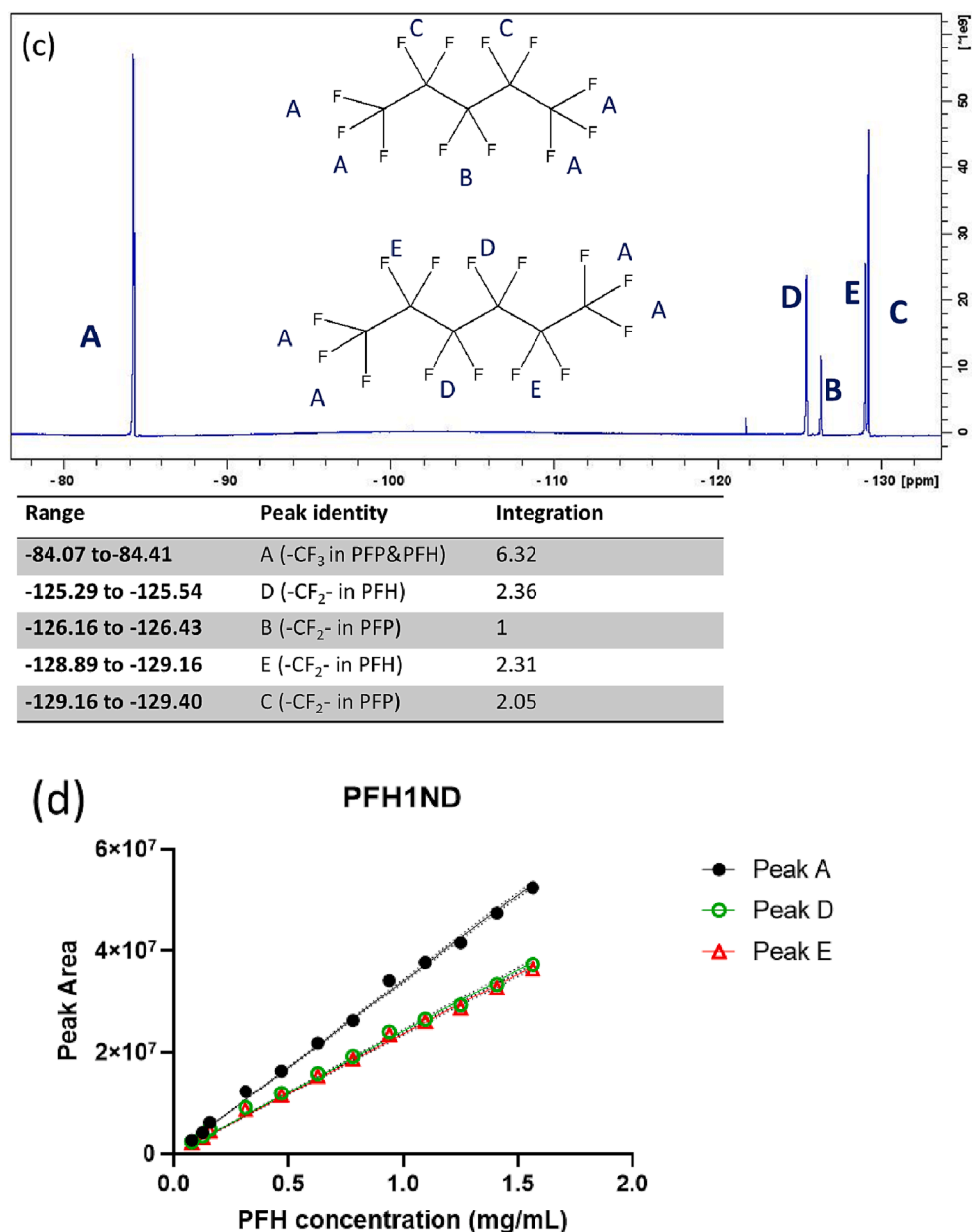The cavitation from NDs was observed using a high-speed camera

Range	Peak identity	Integration
-84.07 to-84.41	A (-CF$_3$ in PFP&PFH)	6.32
-125.29 to -125.54	D (-CF$_2$- in PFH)	2.36
-126.16 to -126.43	B (-CF$_2$- in PFP)	1
-128.89 to -129.16	E (-CF$_2$- in PFH)	2.31
-129.16 to -129.40	C (-CF$_2$- in PFP)	2.05

Fig. 5. (*continued*).

(SV2-9 in SI). Although the syringe containing the diluted microbubble/ND suspension was mechanically agitated between each experiment, we cannot say with certainty that the cavitation observations of Fig. 8 derived from single ND particles. From >200 observations across a range of pressure amplitudes, however, no difference in the cavitation response was noted, that might be attributable to the aggregation of NDs, prior to focused ultrasound incidence. Comparison of the imaging data with Sonazoid® microbubbles under equivalent insonation conditions to that of the different ND compositions (PFP1ND, PFH1ND & MIX1ND), suggests that there is no qualitative difference in the cavitation response from each of the nucleation particles, for all peak negative pressure amplitudes tested. Direct quantitative comparison is prevented by differences in the local values of the pressure fluctuation driving the activity, which will depend on the precise location of the particle within the focus, at the time of ultrasound inception. Fig. 8 shows representative examples of microbubble and ND cavitation at two driving pressure amplitudes. Fig. 8a is at a peak-negative pressure of 0.45 MPa and 8b at a higher peak-negative pressure of 0.73 MPa for which significant

fragmentation occurs. The NDs were observed to cavitate at pressure amplitudes as low as 0.15 MPa, suggesting that these NDs do not require high-pressure amplitudes to vaporise and cavitate. Further studies are required to fully characterise the acoustic behaviour of the NDs, such as during ultrasound imaging [46], ADV threshold measurements [43,47], acoustic emission[48] *etc.*, but the data presented here suggests that the NDs cavitate in a manner comparable to conventional UCA microbubbles. Fig. 9.

3.8. Passive cavitation detection (PCD)

The cavitation activity of PFP1ND, MIX1ND and PFH1ND was monitored using a PCD system at acoustic pressure level between 200 kPa and 1500 kPa with increments of 50 kPa, with degassed buffer as control. The intersection of NDs with control represent the lowest pressure needed for NDs cavitation. The lowest cavitation pressure for all formulations is similar, which is around 400 kPa. There was no significant difference for cavitation energy at 1500 kPa among three NDs
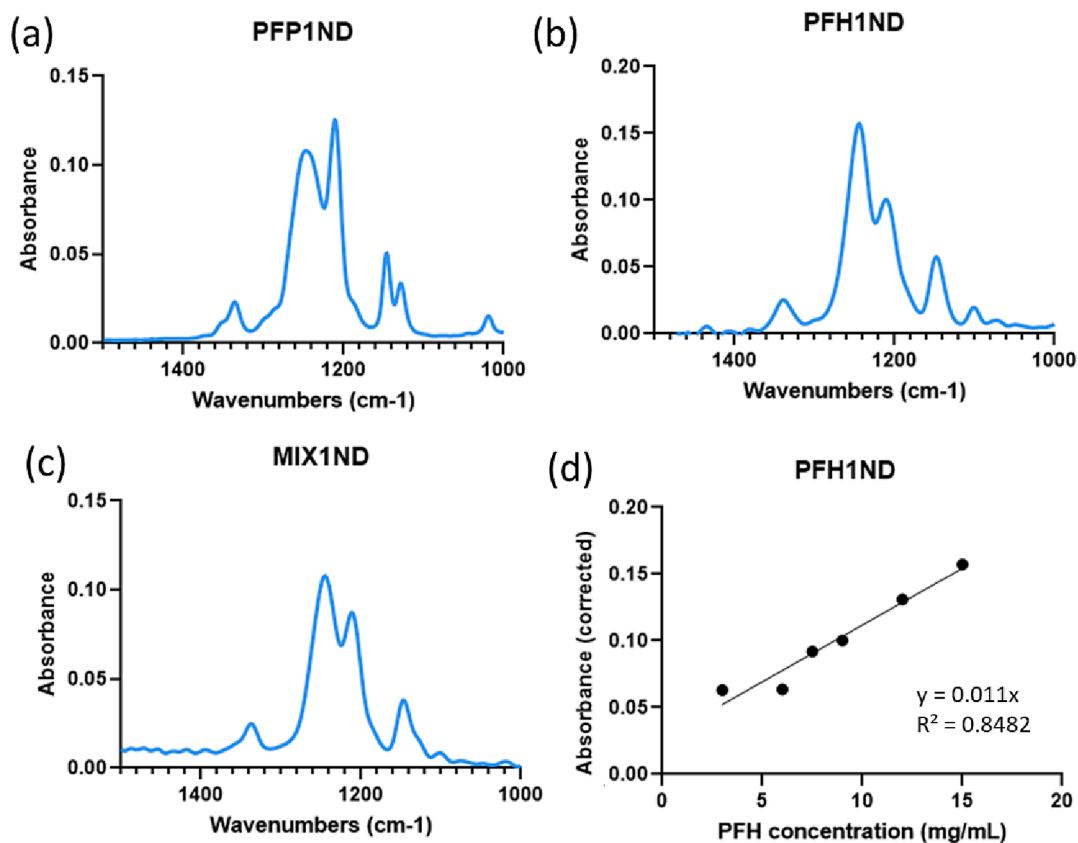
Fig. 6. (a) FTIR spectrum of ND. (a) PFP1ND, (b) PFH1ND, (c) MIX1ND. (d) Correlation between PFH concentration and absorbance. $R^2 = 0.848$ (PFP1ND = ND sample with 1 v/v% PFP as core, MIX1ND = ND sample with 1 v/v% mixture PFC as core, PFH1ND = ND sample with 1% v/v PFH as core).
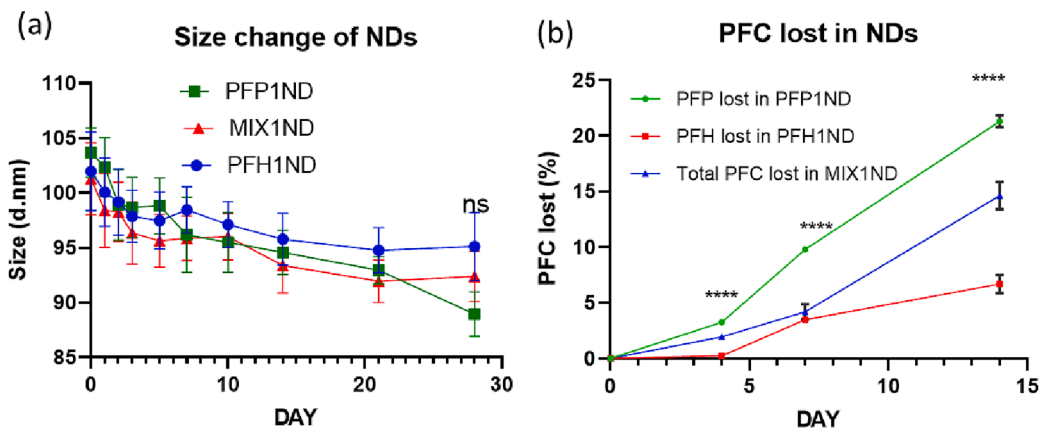

Fig. 7. Stability of NDs during storage. (a) Size change of NDs. For comparison among groups, there were no significant difference among three type of NDs on day 28; (b)Amount of PFC lost in PFP1ND, PFH1ND and MIX1ND (represented as total PFC amount); (PFP1ND = ND sample with 1 v/v% PFP as core, MIX1ND = ND sample with 1 v/v% mixture PFC as core, PFH1ND = ND sample with 1% v/v PFH as core). Data in 7a & 7b are presented as mean ± SD, n = 3. P value was generated by one-way ANOVA test, no significant at $P > 0.05$ (*$P < 0.05$, **$P < 0.01$, ***$P < 0.001$, and ****$P < 0.0001$).

($P > 0.05$), probably due to this is purely a reflection of the resulting microbubble cavitation. These results demonstrated that PFP1ND, MIX1ND and PFH1ND all have cavitation energy, *i.e.* form bubbles, which is important for both imaging and therapeutic application.

In this study we present NDs composed of biodegradable lipid shell and liquid PFC core. The formulated NDs showed a good size around 100–110 nm and size distribution (PDI <0.25). The tumour vascular endothelial gap usually ranges from 380 to 780 nm [49]. Therefore, the size of ND makes them more likely to permeate the tumour blood vessels compared to microbubbles (>3µm). The smaller particle size of our fabricated NDs can help them extravasate out of the tumour vasculature and accumulate in tumour tissue through enhanced the permeability and retention (EPR) effect [50]. After NDs arrive in the tumour, they can be transformed into microbubble and cavitate under ultrasound pressure

[49]. PFC core is the key for NDs ADV and cavitation [51], but previous studies did not explore methods to detect the amount of PFC in ND samples. Therefore, we developed two methods for quantification: ^{19}F NMR and FTIR. Results presented in this study, indicated that ^{19}F NMR is an accurate technique to identify and quantify the encapsulated PFC, and it also has the potential to be used to assess the PFC in biological samples. FTIR lacks quantification accuracy compared with ^{19}F NMR. However, it is a more cost effective and available technique. FTIR could be used to detect NDs' PFC in case the NDs are labelled with magnetic labels, *e.g.* used in imaging. These two methods can help us to assess the stability of NDs samples. In this study, we assessed the stability of NDs using DLS, FTIR and ^{19}F NMR. We confirmed our hypothesis that slight decreases of NDs size was due to PFC leakage. In a previous study, DPPC-based lipid shell microbubbles lost nearly half of its encapsulated O_2 gas
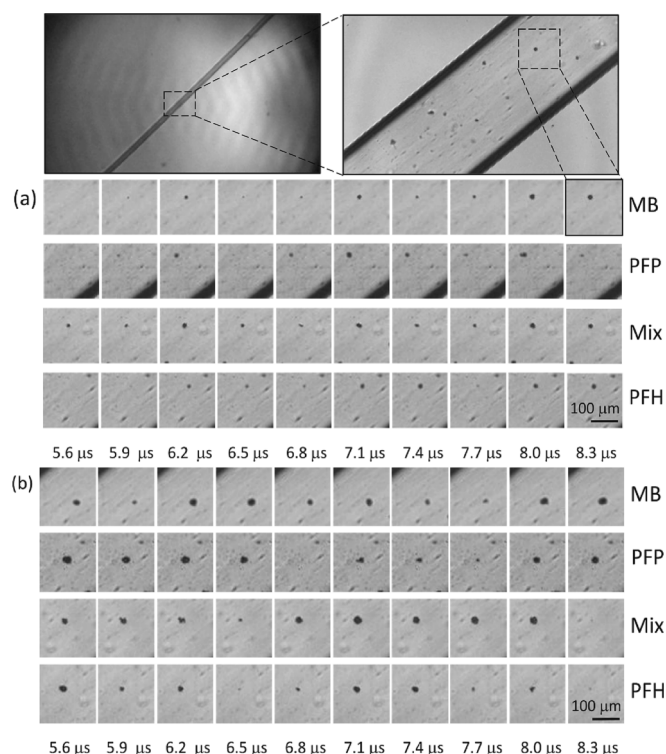
Fig. 8. Representative images of cavitation from MB and NDs under peak negative pressures of (a) 0.45 MPa, (b) 0.73 MPa (PFP = ND sample with 1 v/v % PFP as core, MIX = ND sample with 1 v/v% mixture PFC as core, PFH = ND sample with 1% v/v PFH as core). Full image sequences at full field of view are available as Videos SV2 – SV9 in SI.
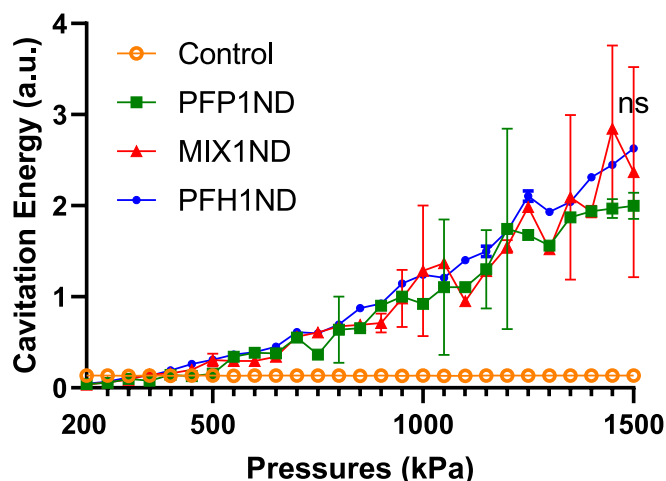
Fig. 9. Cavitation energy of NDs (lipid concentration 1.5 mg/mL) during FUS exposure at various acoustic pressure levels. The following ultrasound parameters were used: 1.5 MHz, 5 Hz PRF, 1500 cycles, 200 kPa- 1500 kPa (50 kPa increments). (PFP1ND = ND sample with 1 v/v% PFP as core, MIX1ND = ND sample with 1 v/v% mixture PFC as core, PFH1ND = ND sample with 1% v/v PFH as core). Data are presented as mean ± SD, n = 100 (100 pulse for each formulation). *P* value was generated by one-way ANOVA test, no significant at $P > 0.05$ (*$P < 0.05$, **$P < 0.01$, ***$P < 0.001$, and ****$P < 0.0001$).

core within a two week storage period [52]. In our studies, PFH NDs lost around 7.6% of its encapsulated liquid PFH within the same period (14 days). Ultrasound was used to trigger phase change of NDs under controlled condition and demonstrate their cavitation response. We observed that NDs do not need high pressure amplitudes to vaporise.

This could avoid the potential adverse effects *in vivo* caused by the application of high acoustic energies [51]. These findings offer the information required to design the shell and choose the right core for stable and acoustically active nanodroplets.

4. Conclusions

Lipid-shell NDs were formulated using three different core compositions, following an optimised bath-sonication method. Their physicochemical properties were assessed. The NDs showed an acceptable small size and homogeneous size distribution that could be used for future tumour permeation applications. Size was maintained under storage conditions. We have developed two methods to quantify the PFC core of the NDs using ^{19}F NMR and FTIR. Monitoring PFC levels will help monitor the stability and performance of phase change NDs. Our fabricated NDs do not require high pressure amplitudes to vaporise and cavitate, which shows they have great potential to be used as ultrasound contrast agents.

Declaration of Competing Interest

The authors declare that they have no known competing financial interests or personal relationships that could have appeared to influence the work reported in this paper.

Appendix A. Supplementary data

Supplementary data to this article can be found online at https://doi.org/10.1016/j.ultsonch.2023.106445.

References

[1] K.H. Martin, P.A. Dayton, Current status and prospects for microbubbles in ultrasound theranostics, Wiley Interdiscip. Rev. Nanomedicine Nanobiotechnology 5 (4) (2013) 329–345.

[2] Z. Fan, R.E. Kumon, C.X. Deng, Mechanisms of microbubble-facilitated sonoporation for drug and gene delivery, Ther. Deliv. 5 (2014) 467–486.

[3] M.F. Meloni, et al., Radiofrequency ablation of liver tumors: the role of microbubble ultrasound contrast agents, Ultrasound Q. 22 (2006) 41–47.

[4] S.R. Sirsi, M.A. Borden, Microbubble compositions, properties and biomedical applications, Bubble Sci. Eng. & Technol. 1 (1-2) (2009) 3–17.

[5] K. Loskutova, D. Grishenkov, M. Ghorbani, Review on Acoustic Droplet Vaporization in Ultrasound Diagnostics and Therapeutics, Biomed Res. Int. 2019 (2019) 1–20.

[6] C.C. Chen, P.S. Sheeran, S.-Y. Wu, O.O. Olumolade, P.A. Dayton, E.E. Konofagou, Targeted drug delivery with focused ultrasound-induced blood-brain barrier opening using acoustically-activated nanodroplets, J. Control. Release 172 (3) (2013) 795–804.

[7] E. Stride, et al., Microbubble Agents: New Directions, Ultrasound Med. Biol. 46 (2020) 1326–1343.

[8] R. Guo, et al., Functional ultrasound-triggered phase-shift perfluorocarbon nanodroplets for cancer therapy, Ultrasound Med. Biol. 47 (2021) 2064–2079.

[9] A. Ishijima, J. Tanaka, T. Azuma, K. Minamihata, S. Yamaguchi, E. Kobayashi, T. Nagamune, I. Sakuma, The lifetime evaluation of vapourised phase-change nano-droplets, Ultrasonics 69 (2016) 97–105.

[10] M.A. Borden, G. Shakya, A. Upadhyay, K.H. Song, Acoustic nanodrops for biomedical applications, Curr. Opin. Colloid Interface Sci. 50 (2020), 101383.

[11] C. Mannaris, et al., Microbubbles, Nanodroplets and Gas-Stabilizing Solid Particles for Ultrasound-Mediated Extravasation of Unencapsulated Drugs: An Exposure Parameter Optimization Study, Ultrasound Med. Biol. 45 (2019) 954–967.

[12] S.K. Yarmoska, H. Yoon, S.Y. Emelianov, Lipid Shell Composition Plays a Critical Role in the Stable Size Reduction of Perfluorocarbon Nanodroplets, Ultrasound Med. Biol. 45 (2019) 1489–1499.

[13] A.L.Y. Kee, B.M. Teo, Biomedical applications of acoustically responsive phase shift nanodroplets: Current status and future directions, Ultrason. Sonochem. 56 (2019) 37–45.

[14] P.S. Sheeran, T.O. Matsunaga, P.A. Dayton, Phase-transition thresholds and vaporization phenomena for ultrasound phase-change nanoemulsions assessed via high-speed optical microscopy, Phys. Med. Biol. 58 (2013) 4513–4534.

[15] W. Zhang, Y. Shi, S. Abd Shukor, A. Vijayakumaran, S. Vlatakis, M. Wright, M. Thanou, Phase-shift nanodroplets as an emerging sonoresponsive nanomaterial for imaging and drug delivery applications, Nanoscale 14 (8) (2022) 2943–2965.

[16] N. Rapoport, Z. Gao, A. Kennedy, Multifunctional nanoparticles for combining ultrasonic tumor imaging and targeted chemotherapy, J. Natl. Cancer Inst. 99 (2007) 1095–1106.

[17] H. Lea-Banks, M.A. O'Reilly, K. Hynynen, Ultrasound-responsive droplets for therapy: A review, J. Control. Release 293 (2019) 144–154.

[18] P.S. Sheeran, T.O. Matsunaga, P.A. Dayton, Phase change events of volatile liquid perfluorocarbon contrast agents produce unique acoustic signatures, Phys. Med. Biol. 59 (2014) 379–401.

[19] N. Rapoport, K.-H. Nam, R. Gupta, Z. Gao, P. Mohan, A. Payne, N. Todd, X. Liu, T. Kim, J. Shea, C. Scaife, D.L. Parker, E.-K. Jeong, A.M. Kennedy, Ultrasound-mediated tumor imaging and nanotherapy using drug loaded, block copolymer stabilized perfluorocarbon nanoemulsions, J. Control. Release 153 (1) (2011) 4–15.

[20] R. Melich, et al., Microfluidic preparation of various perfluorocarbon nanodroplets: Characterization and determination of acoustic droplet vaporization (ADV) threshold, Int. J. Pharm. 587 (2020), 119651.

[21] J.Y. Lee, C. Crake, B. Teo, D. Carugo, M. de Saint Victor, A. Seth, E. Stride, Ultrasound-Enhanced siRNA Delivery Using Magnetic Nanoparticle-Loaded Chitosan-Deoxycholic Acid Nanodroplets, Adv. Healthc. Mater. 6 (8) (2017) 1601246.

[22] J.S. Harmon, et al., Gas embolization in a rodent model of hepatocellular carcinoma using acoustic droplet vaporization, in: in *2018 40th Annual International Conference of the IEEE Engineering in Medicine and Biology Society (EMBC)*, (IEEE, 2018, pp. 6048–6051.

[23] K. Kawabata, R. Asami, T. Azuma, S. Umemura, Acoustic response of microbubbles derived from phase-change nanodroplet, Jpn. J. Appl. Phys. 49 (2010) 07HF18.

[24] P. Zhang, T. Porter, An in vitro study of a phase-shift nanoemulsion: a potential nucleation agent for bubble-enhanced HIFU tumor ablation, Ultrasound Med. Biol. 36 (2010) 1856–1866.

[25] N. Chang, et al., Efficient and controllable thermal ablation induced by short-pulsed HIFU sequence assisted with perfluorohexane nanodroplets, Ultrason. Sonochem. 45 (2018) 57–64.

[26] E. Vlaisavljevich, Y.Y. Durmaz, A. Maxwell, M. ElSayed, Z. Xu, Nanodroplet-mediated histotripsy for image-guided targeted ultrasound cell ablation, Theranostics 3 (11) (2013) 851–864.

[27] K. Astafyeva, et al., Perfluorocarbon nanodroplets stabilized by fluorinated surfactants: Characterization and potentiality as theranostic agents, J. Mater. Chem. B 3 (2015) 2892–2907.

[28] C. Mannaris, et al., Acoustically responsive polydopamine nanodroplets: A novel theranostic agent, Ultrason. Sonochem. 60 (2020), 104782.

[29] F. Baghbani, et al., Formulation design, preparation and characterization of multifunctional alginate stabilized nanodroplets, Int. J. Biol. Macromol. 89 (2016) 550–558.

[30] S. Ferri, et al., Tailoring the size of ultrasound responsive lipid-shelled nanodroplets by varying production parameters and environmental conditions, Ultrason. Sonochem. 73 (2021), 105482.

[31] R. Asami, T. Ikeda, T. Azuma, S. Umemura, K.-I. Kawabata, & Ken-Ichi Kawabata. Acoustic signal characterization of phase change nanodroplets in tissue-mimicking phantom gels, Jpn. J. Appl. Phys. 49 (7S) (2010) 07HF16.

[32] S. Xu, et al., Acoustic droplet vaporization and inertial cavitation thresholds and efficiencies of nanodroplets emulsions inside the focused region using a dual-frequency ring focused ultrasound, Ultrason. Sonochem. 48 (2018) 532–537.

[33] T. Lacour, M. Guédra, T. Valier-Brasier, F. Coulouvrat, A model for acoustic vaporization dynamics of a bubble/droplet system encapsulated within a hyperelastic shell, J. Acoust. Soc. Am. 143 (2018) 23–37.

[34] P.S. Sheeran, P.A. Dayton, Improving the Performance of Phase-Change Perfluorocarbon Droplets for Medical Ultrasonography: Current Progress, Challenges, and Prospects, Scientifica (Cairo). 2014 (2014) 1–24.

[35] Y. Yang, D. Yang, Q.i. Zhang, X. Guo, J.L. Raymond, R.A. Roy, D. Zhang, J. Tu, The influence of droplet concentration on phase change and inertial cavitation thresholds associated with acoustic droplet vaporization, J. Acoust. Soc. Am. 148 (4) (2020) EL375. EL381.

[36] J.D. Rojas, M.A. Borden, P.A. Dayton, Effect of Hydrostatic Pressure, Boundary Constraints and Viscosity on the Vaporization Threshold of Low-Boiling-Point Phase-Change Contrast Agents, Ultrasound Med. Biol. 45 (2019) 968–979.

[37] Johansen, K., Song, J. H. & Prentice, P. Characterising focused ultrasound via high speed shadowgraphic imaging at 10 million frames per second. *IEEE Int. Ultrason. Symp. IUS* **2016**-Novem. 8–11. (2016).

[38] A.N. Pouliopoulos, et al., Temporal Stability of Lipid-Shelled Microbubbles During Acoustically-Mediated Blood-Brain Barrier Opening, Front. Phys. 8 (2020) 1–16.

[39] Ruozi, B. *et al.* AFM, ESEM, TEM, and CLSM in liposomal characterization: a comparative study. *Int. J. Nanomedicine.* 557–563. (2011).

[40] Z. Gao, A.M. Kennedy, D.A. Christensen, N.Y. Rapoport, Drug-loaded nano/microbubbles for combining ultrasonography and targeted chemotherapy, Ultrasonics 48 (4) (2008) 260–270.

[41] P.S. Sheeran, et al., Methods of generating submicrometer phase-shift perfluorocarbon droplets for applications in medical ultrasonography, IEEE Trans. Ultrason. Ferroelectr. Freq. Control 64 (2017) 252–263.

[42] S. Santra, C. Kaittanis, J. Grimm, J.M. Perez, Drug/dye-loaded, multifunctional iron oxide nanoparticles for combined targeted cancer therapy and dual optical/magnetic resonance imaging, Small 5 (16) (2009) 1862–1868.

[43] Q. Wu, et al., Investigation of the acoustic vaporization threshold of lipid-coated perfluorobutane nanodroplets using both high-speed optical imaging and acoustic methods, Ultrasound Med. Biol. 47 (2021) 1826–1843.

[44] A. Hannah, G. Luke, K. Wilson, K. Homan, S. Emelianov, Indocyanine green-loaded photoacoustic nanodroplets: Dual contrast nanoconstructs for enhanced photoacoustic and ultrasound imaging, ACS Nano 8 (1) (2014) 250–259.

[45] H. Choi, W. Choi, J. Kim, W.H. Kong, K.S. Kim, C. Kim, S.K. Hahn, Multifunctional Nanodroplets Encapsulating Naphthalocyanine and Perfluorohexane for Bimodal Image-Guided Therapy, Biomacromolecules 20 (10) (2019) 3767–3777.

[46] S. Lin, G.e. Zhang, A. Jamburidze, M. Chee, C.H. Leow, V. Garbin, M.-X. Tang, Imaging of vaporised sub-micron phase change contrast agents with high frame rate ultrasound and optics, Phys. Med. Biol. 63 (6) (2018) 065002.

[47] F. Dong, J. An, J. Zhang, J. Yin, W. Guo, D.i. Wang, F. Feng, S. Huang, J. Zhang, H. Cheng, Blinking acoustic nanodroplets enable fast super-resolution ultrasound imaging, ACS Nano 15 (10) (2021) 16913–16923.

[48] J.H. Song, A. Moldovan, P. Prentice, Non-linear Acoustic Emissions from Therapeutically Driven Contrast Agent Microbubbles, Ultrasound Med. Biol. 45 (2019) 2188–2204.

[49] H. Yang, et al., A new strategy for accurate targeted diagnosis and treatment of cutaneous malignant melanoma: dual-mode phase-change lipid nanodroplets as ultrasound contrast agents, Int. J. Nanomedicine 14 (2019) 7079–7093.

[50] P.S. Sheeran, P.A. Dayton, Phase-change contrast agents for imaging and therapy, Curr. Pharm. Des. 18 (2012) 2152–2165.

[51] P.G. Durham, P.A. Dayton, Applications of sub-micron low-boiling point phase change contrast agents for ultrasound imaging and therapy, Curr. Opin. Colloid Interface Sci. 56 (2021), 101498.

[52] E.J. Swanson, V. Mohan, J. Kheir, M.A. Borden, Phospholipid-stabilized microbubble foam for injectable oxygen delivery, Langmuir 26 (20) (2010) 15726–15729.